Global neutrino data and recent reactor fluxes: the status of three-flavour oscillation parameters

2011 New J. Phys. 13 063004

(http://iopscience.iop.org/1367-2630/13/6/063004)

New Journal of Physics
The open-access journal for physics

Global neutrino data and recent reactor fluxes: the status of three-flavour oscillation parameters

Thomas Schwetz[1], **Mariam Tórtola**[2] **and J W F Valle**[2]

[1] Max-Planck-Institut für Kernphysik, PO Box 103980, 69029 Heidelberg, Germany

[2] AHEP Group, Instituto de Física Corpuscular—CSIC/Universitat de València, Edificio Institutos de Paterna, Apt 22085, E-46071 Valencia, Spain

E-mail: schwetz@mpi-hd.mpg.de, mariam@ific.uv.es and valle@ific.uv.es

New Journal of Physics **13** (2011) 063004 (15pp)
Received 14 March 2011
Published 1 June 2011
Online at http://www.njp.org/
doi:10.1088/1367-2630/13/6/063004

Abstract. We present the results of a global neutrino oscillation data analysis within the three-flavour framework. We include the latest results from the MINOS long-baseline experiment (including electron neutrino appearance and anti-neutrino data), updating all relevant solar (Super-Kamiokande (SK) II + III), atmospheric (SK I + II + III) and reactor (KamLAND) data. Furthermore, we include a recent re-calculation of the anti-neutrino fluxes emitted from nuclear reactors. These results have important consequences for the analysis of reactor experiments and in particular for the status of the mixing angle θ_{13}. In our recommended default analysis, we find from the global fit that the hint for nonzero θ_{13} remains weak, at 1.8σ for both neutrino mass hierarchy schemes. However, we discuss in detail the dependence of these results on assumptions regarding the reactor neutrino analysis.

Contents

1. Introduction

The discovery of neutrino mixing and oscillations provides strong evidence for physics beyond the Standard Model, opening a new era in particle physics. Here we update the three-neutrino oscillation results of [1][3] with a special emphasis on the new reactor anti-neutrino flux results of [5, 6], which have an important impact on the determination of the mixing angle θ_{13}. We include new data from the MINOS Collaboration, both for $\nu_\mu \to \nu_e$ transitions [7] and ν_μ disappearance [8–10], the latest super-Kamiokande (SK) solar [11, 12] and atmospheric [13] neutrino data, as well as recent KamLAND reactor data [14]. Our goal is to summarize the results of the three-flavour neutrino oscillation analysis paying attention to sub-leading three-flavour effects where they are most relevant, as well as to the effects of the new anti-neutrino flux emitted from nuclear reactors, which has been re-evaluated in [5]. The reported value of the $\bar{\nu}_e$ flux is about 3% higher than that from previous calculations. This has important consequences for the interpretation of data from reactor experiments. We discuss the implications of the new reactor neutrino flux for the determination of oscillation parameters, in particular its effect on the mixing angle θ_{13}. We find that due to the new fluxes the results depend on the inclusion of short-baseline (SBL) reactor data from distances $\lesssim$100 m.

In section 2, we present the updated analysis in the 'atmospheric sector', discussing the SK I+II+III data [13] in section 2.1 and the MINOS disappearance results, taking into account the solar squared-mass splitting and discussing the slight tension between neutrino and anti-neutrino data, in section 2.2. In section 2.3, we focus on the combined SK+MINOS analysis and the determination of θ_{13} from these data. Section 3 contains a discussion on the reactor neutrino data in light of the new predicted anti-neutrino fluxes; in section 4, we discuss solar neutrino data, as well as KamLAND and the other reactor experiments. The results of the global fit are summarized in section 5, which includes a detailed discussion on the status of θ_{13}. In particular, we discuss the dependence of the θ_{13} determination on assumptions regarding the reactor anti-neutrino data analysis. The conclusions are presented in section 6.

[3] When referring to this paper we include also its updates available at arXiv:0808.2016v3 [hep-ph]. Further technical details of the analysis as well as earlier experimental references are also given in our previous review [2]. For other global analyses, see [3, 4].

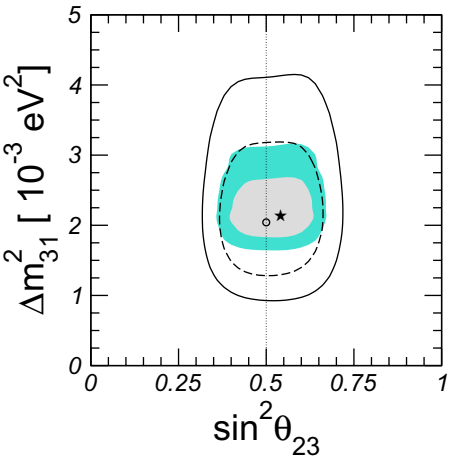

Figure 1. Comparison of our previous SK-I atmospheric analysis (empty regions) and the new analysis using the latest atmospheric data from SK-I, SK-II and SK-III (shaded regions) for inverted mass hierarchy. Best-fit points are indicated by a dot and a star, respectively.

2. The atmospheric sector: Super-Kamiokande (SK) I+II+III and MINOS

2.1. SK I + II + III data

We include in our analysis the full sample of atmospheric neutrino data from all three phases of the SK experiment [13], using directly the χ^2 map provided by the SK collaboration. The atmospheric neutrino oscillation analysis is performed within the one mass scale approximation, neglecting the effect of the solar mass splitting, as in our previous papers [1, 2][4].

In figure 1, we show the results of our previous atmospheric neutrino analysis in [1, 2] including data from the first phase of the SK experiment, compared with the new analysis included in this update, based on the SK data from all three phases of the experiment. The differences between the two analyses are clearly seen, with an improved determination of both the oscillation parameters. As we will see in the following, once data from neutrino disappearance at the MINOS long-baseline experiments are included in the analysis, the improvement in the determination of Δm^2_{31} due to the recent atmospheric neutrino data is 'hidden' by the more constraining restrictions imposed by long-baseline data. Nevertheless, this new atmospheric analysis will be important when constraining the mixing angle θ_{23} and also θ_{13}.

2.2. MINOS disappearance data

At the Neutrino 2010 Conference, the MINOS Collaboration presented new data from their searches for ν_μ disappearance, both from the neutrino (7.2×10^{20} protons-on-target (p.o.t.)) and the anti-neutrino (1.71×10^{20} p.o.t.) running mode. The neutrino analysis uses 27 energy bins between 0 and 10 GeV, whereas in the case of anti-neutrinos the data sample is given as 13

[4] Preliminary results towards a full three-flavour atmospheric neutrino analysis are presented in [15]; we look forward to the corresponding information becoming publicly available.

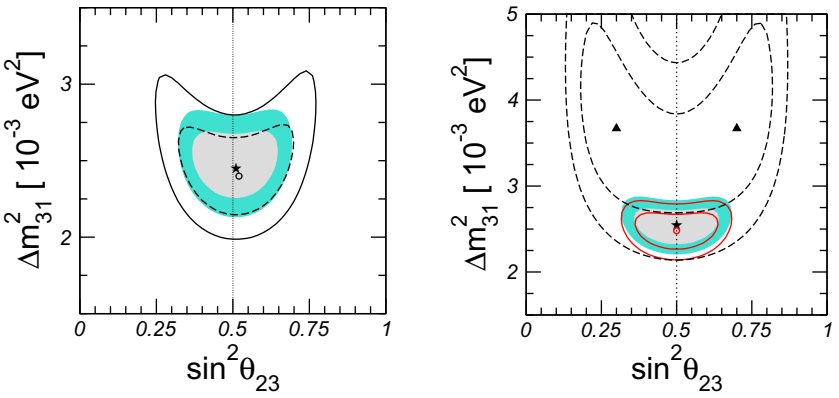

Figure 2. Determination of atmospheric neutrino parameters by the MINOS long-baseline experiment at 90% CL and 3σ. Left panel: the previous (3.36×10^{20} p.o.t., empty regions) versus current (7.2×10^{20} p.o.t., coloured/shaded regions) ν_μ data. Right panel: the allowed regions from recent MINOS (7.2×10^{20} p.o.t.) data, using neutrinos-only (red/solid empty lines), anti-neutrinos-only (black/dashed empty lines) and the combination (coloured/shaded regions). Both panels assume normal hierarchy. Best-fit points follow the same colour code.

energy bins in the range between 0 and 30 GeV. We perform a re-analysis of the data from [8–10] within a full three-flavour framework using GLoBES software [16] to simulate the experiment. In our analysis we include the backgrounds provided by the MINOS collaboration, assuming a total systematic uncertainty of 5%. For neutrinos we assume an energy resolution of 15%, whereas for anti-neutrinos we take the width of the energy resolution to be $0.1E_\nu + 0.15\sqrt{E_\nu}$ for E_ν in GeV. With this choice of energy resolutions, one can reproduce well the two-flavour allowed regions obtained by MINOS. In addition to matter effects, we include also the effect of Δm^2_{21} as well as θ_{13} and the CP-phase δ in the analysis of the disappearance and appearance channels. Since in our analysis MINOS data are the only ones sensitive to the phase δ we always minimize the MINOS χ^2 with respect to δ.

In figure 2, the analysis of the new MINOS data is compared with the previous data release (left panel). Apart from the smaller size of the allowed regions due to an increase in statistics, we notice also a change in shape of the regions. This follows from the inclusion of the sub-leading three-flavour effects in this new analysis.

In the right panel, we illustrate the impact of the (still small) anti-neutrino sample. From this figure, it can be seen that there is a slight tension between the neutrino and the anti-neutrino results: there is no overlap of the allowed regions at less than 90% CL. However, at 3σ the results of both are fully consistent. We find the following χ^2 minima and goodness-of-fit (GOF) values:

$$\begin{aligned} \nu: &\quad \chi^2_{\mathrm{min},\nu} = 24.4/(27-2), \ \mathrm{GOF} = 49.6\%, \\ \bar{\nu}: &\quad \chi^2_{\mathrm{min},\bar{\nu}} = 15.0/(13-2), \ \mathrm{GOF} = 18.4\%, \\ \nu+\bar{\nu}: &\quad \chi^2_{\mathrm{min,tot}} = 46.1/(40-2), \ \mathrm{GOF} = 17.3\%. \end{aligned} \tag{1}$$

Hence, the combined neutrino and anti-neutrino fit still provides an acceptable GOF. Using the consistency test of [17] yields $\chi^2_{\mathrm{PG}} = \chi^2_{\mathrm{min,tot}} - \chi^2_{\mathrm{min},\nu} - \chi^2_{\mathrm{min},\bar{\nu}} = 6.7$. The value of χ^2_{PG} must be

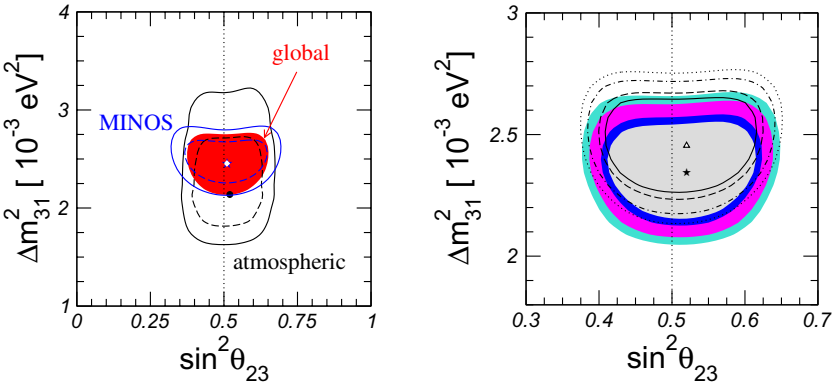

Figure 3. Determination of the atmospheric oscillation parameters. Left: the interplay of atmospheric (black) and MINOS disappearance (blue) data and the combination (red/shaded region) for normal hierarchy at 90% CL (dashed) and 3σ (solid). Right: the combined allowed regions for normal (black curves) and inverted hierarchy (coloured regions) at 90, 95, 99 and 99.73% CL.

evaluated for two degrees of freedom, which implies that the neutrino and the anti-neutrino data are consistent with a probability of 3.7%. This number indicates a slight tension between the sets, at the level of about 2.1σ. In the following, we will use only neutrino data in the global analysis. It is clear from figure 2 (right) that including also anti-neutrino data would have a negligible impact on the global result.

2.3. The atmospheric sector: combined MINOS + atmospheric analysis and θ_{13}

Combining the new atmospheric and MINOS disappearance data, we obtain new global constraints on the atmospheric neutrino oscillation parameters. The results are shown in figure 3. As before, Δm^2_{31} is determined mainly by the MINOS data, whereas the atmospheric data are more important in determining the mixing parameter $\sin^2\theta_{23}$. Note that the sub-leading effects of Δm^2_{21} lead to different best-fit points for $|\Delta m^2_{31}|$, depending on whether the mass hierarchy is normal (NH) or inverted (IH). We find the following best-fit values with errors at 1σ:

$$|\Delta m^2_{31}| = \begin{cases} 2.45 \pm 0.09 & \times 10^{-3}\,\text{eV}^2 \quad \text{(NH)}, \\ 2.34^{+0.10}_{-0.09} & \times 10^{-3}\,\text{eV}^2 \quad \text{(IH)}. \end{cases} \tag{2}$$

The corresponding allowed regions are shown in figure 3 (right). The reason for this apparent shift is just a result of our parameterization, using Δm^2_{31} for both hierarchies, and changing only its sign to cover the two cases. Hence, in NH the 'largest' frequency is given by $|\Delta m^2_{31}|$, whereas in IH it is $|\Delta m^2_{31}| + \Delta m^2_{21}$, which explains why $|\Delta m^2_{31}|$ is smaller for IH. Equation (2) shows that these sub-leading effects must be included given the present accuracy, since they are at the level of the 1σ error on Δm^2_{31}.

Now we move on to the MINOS appearance data. Recently the MINOS Collaboration has also reported new data from the search for $\nu_\mu \to \nu_e$ transitions in the Fermilab NuMI beam [7]. The new data are based on a total exposure of 7×10^{20} p.o.t, more than twice the size of the previous data release [18]. The new MINOS far detector data consist of 54 electron neutrino events, whereas, according to the measurements in the MINOS near detector,

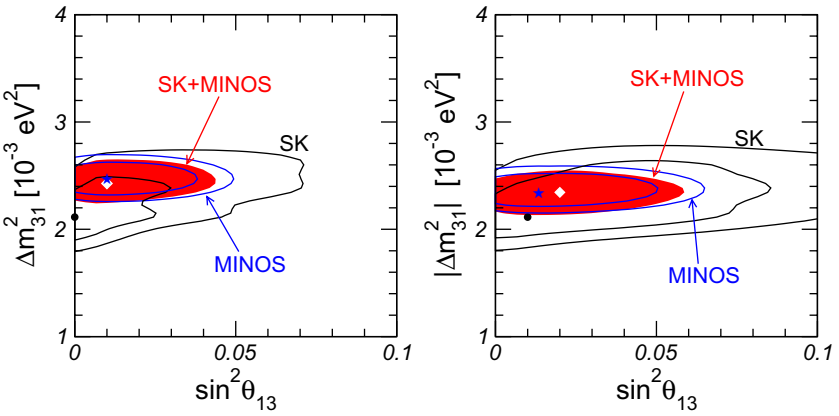

Figure 4. Allowed regions at 1σ and 90% CL for atmospheric (SK) and MINOS disappearance and appearance data in the plane of $\sin^2\theta_{13}$ and Δm^2_{31} for NH (left) and IH (right). Combined data are shown as shaded/red region at 90% CL. The black dot, blue star and white diamond correspond to the best-fit points of SK, MINOS and SK+MINOS, respectively.

$49.1 \pm 7.0(\text{stat}) \pm 2.7(\text{syst})$ background events were expected. Hence, the observed number of events is in agreement with background expectations within 0.7σ, and the hint for a nonzero value of θ_{13} present in previous data [18] has largely disappeared. In fact, we see that once we include the new MINOS data in our analysis, a smaller best-fit point of θ_{13} is obtained. As a result, the hint for θ_{13} is less significant than before: for both hierarchies we find only a 0.8σ hint when using the new MINOS data versus 1.3σ obtained with the previous MINOS appearance data; for a discussion see, e.g., [19].

The atmospheric neutrino data from SK I + II + III described in the previous section imply a best-fit point very close to $\theta_{13} = 0$ [13], with $\Delta\chi^2 = 0.0(0.3)$ for $\theta_{13} = 0$ for NH (IH). However, in the combination of MINOS disappearance and appearance data, we even find a slight preference for $\theta_{13} > 0$, with $\Delta\chi^2 = 1.6(1.9)$ at $\theta_{13} = 0$ for NH (IH). As shown in figure 4, this happens due to a small mismatch of the best-fit values for $|\Delta m^2_{31}|$ at $\theta_{13} = 0$, which can be resolved by allowing nonzero values of θ_{13} [3]. This is similar to the hint for $\theta_{13} > 0$ coming from a slight tension between solar and KamLAND data; see [1, 2, 20, 21]. Therefore, the hint for $\theta_{13} > 0$ from the atmospheric+LBL data is now slightly stronger than the one obtained with previous data.

3. New reactor fluxes and implications for oscillation parameters

Until very recently, the interpretation of neutrino oscillation searches at nuclear power plants was based on calculations of the reactor $\bar{\nu}_e$ flux given in [22, 23]. Indeed, the observed rates at all reactor experiments performed so far at distances $L \lesssim 1$ km are consistent with these fluxes, therefore setting limits on $\bar{\nu}_e$ disappearance. Recently, the flux of $\bar{\nu}_e$ emitted from nuclear power plants was re-evaluated [5], yielding roughly 3% higher neutrino fluxes than assumed previously. As discussed in [6], this might indicate an anomaly in reactor experiments at $L \lesssim 1$ km, which according to the new fluxes observe a slight deficit. For the Chooz and Palo Verde experiments at $L \simeq 1$ km, a nonzero θ_{13} could lead to $\bar{\nu}_e$ disappearance accounting for

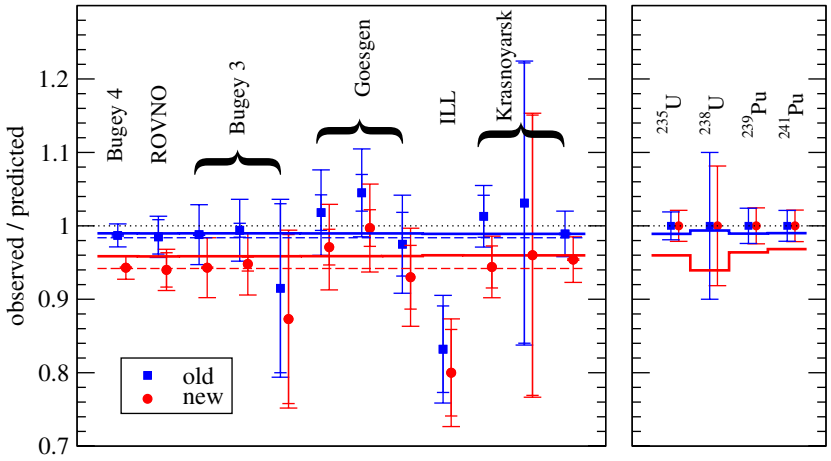

Figure 5. SBL reactor data. We show the observed rate relative to the predicted rate based on old [22] (blue) and new [5, 6] (red) flux calculations. Small error bars show statistical and uncorrelated systematic uncertainties; large error bars include, in addition, correlated systematic Al uncertainties. The solid histograms correspond to the fitted prediction shifted due to the uncertainty on the fluxes [6], as indicated in the right panel. The dashed lines show the best fit assuming a free overall normalization of reactor fluxes. See the text for details.

the reduction in the rate. However, Δm^2_{13} and θ_{13} driven oscillations will have no effect on SBL experiments with $L \lesssim 100$ m.

Motivated by this situation, we include here the SBL reactor experiments Bugey4 [24], ROVNO [25], Bugey3 [26], Krasnoyarsk [27], ILL [28] and Gösgen [29] via the rate measurements summarized in table 2 of [6], in addition to the fit of the KamLAND, Chooz [30] and Palo Verde [31] experiments. We use the neutrino fluxes from the isotopes ^{235}U, ^{239}Pu, ^{238}U and ^{241}Pu given in [5]. For each reactor experiment we take into account the appropriate relative contribution of the isotopes to the total flux and we include the uncertainty on the integrated flux for each isotope given in table 1 of [6], correlated among all experiments. The total error on fluxes from ^{235}U, ^{239}Pu and ^{241}Pu are at the level of 2%, where we assume that an error of 1.8% is fully correlated among the three isotopes, due to a common normalization uncertainty of the corresponding beta-spectra measured in [22].

The SBL reactor data are summarized in figure 5. We show the observed rate relative to the predicted rate based on old and new flux calculations. Due to the slightly higher fluxes according to [5] all experiments observe a smaller ratio with the new fluxes. In figure 5, we show also the result of a fit to the data with the predicted fluxes, allowing the four neutrino fluxes to float in the fit subject to the uncertainties as described above. In the fit we assume that the experimental systematic errors of the three data points from Bugey3, Gösgen and Krasnoyarsk, as well as Bugey4 and ROVNO, are correlated, due to the same experimental technique. We obtain $\chi^2 = 8.1$ (13.0) for 12 degrees of freedom using old (new) fluxes. Clearly old fluxes provide a better fit to the data, whereas the χ^2 for new fluxes is still acceptable (P-value of 37%). Such a good fit can be obtained by a rescaling of the fluxes (subject to the quoted uncertainties) as shown in the right panel.

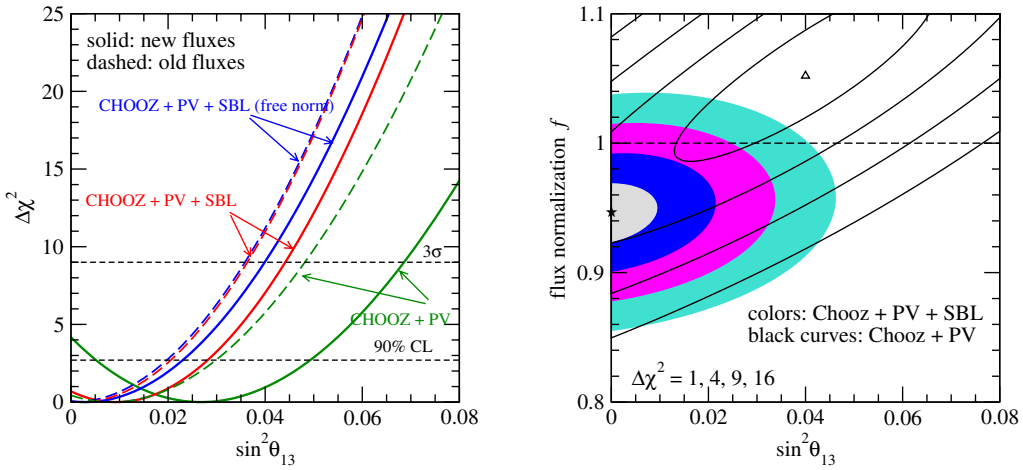

Figure 6. Left: $\Delta\chi^2$ as a function of $\sin^2\theta_{13}$ for the Chooz and Palo Verde (PV) reactor experiments (green), and in combination with the SBL experiments from figure 5. Solid (dashed) curves refer to the new (old) reactor anti-neutrino fluxes. For the blue curves ('free norm'), a free overall normalization factor has been introduced for the reactor fluxes. In this figure we fix $\Delta m^2_{31} = 2.45 \times 10^{-3}\,\mathrm{eV}^2$. Right: contours in the plane of $\sin^2\theta_{13}$ and the flux normalization f. Coloured regions (curves) correspond to Chooz + PV with (without) the inclusion of the SBL experiments.

The dashed lines in the figure correspond to a fit where we introduce an overall factor f in front of the fluxes, which we let float freely in the fit. For the old fluxes, we find the best fit value of $f = 0.984$ with $f = 1$ within the 1σ range. In contrast, for new fluxes we obtain $f = 0.942 \pm 0.024$, and $f = 1$ disfavoured with $\Delta\chi^2 = 6.2$, which corresponds to about 2.5σ. This is the origin of the 'reactor anti-neutrino anomaly' discussed in [6]. A possible explanation of this anomaly could be the presence of a sterile neutrino 'visible' in this oscillation channel but not in the solar and/or atmospheric conversions, the so-called $3+1$ scenario; see, e.g., [32]. However, within the uncertainties on the neutrino flux prediction, the GOF of the new fluxes to SBL reactor data is still rather good. Given this somewhat ambiguous situation, in the following we will present the results for three-flavour oscillations adopting different assumptions regarding reactor neutrino fluxes: (a) motivated by the excellent GOF of SBL data to the new flux prediction, we take fluxes and the quoted uncertainties at face value, and (b) we introduce the free flux normalization f in the fit. This second option takes into account the possible presence of a sterile neutrino or some other correlated effect on all reactor neutrino fluxes. In this scenario, the SBL reactor experiments effectively serve as near detectors determining the flux, which is then used as input for the oscillation analysis at longer baselines.

We show the $\Delta\chi^2$ from the Chooz and Palo Verde experiments as a function of $\sin^2\theta_{13}$ in figure 6 (left) for various assumptions regarding the fluxes. If the new fluxes are taken at face value and SBL reactor experiments are not included in the fit (solid green curve), we obtain from Chooz and Palo Verde a hint for $\theta_{13} > 0$ at about 90% CL, with a best-fit value at $\sin^2\theta_{13} = 0.021$. In this case, $\bar{\nu}_e$ disappearance due to θ_{13} accounts for the suppression of the observed rate at $L \simeq 1\,\mathrm{km}$ relative to the slightly increased prediction from the new fluxes. However, as soon as SBL reactor experiments are included in the fit, the hint essentially

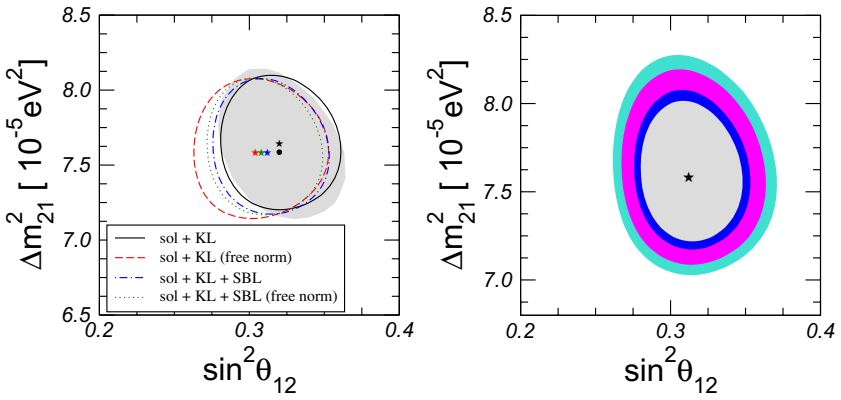

Figure 7. Left: 2σ allowed regions in the $\sin^2\theta_{12}$–Δm^2_{21} plane from the analysis of solar + KamLAND data minimizing over θ_{13}. The different curves show the results obtained using different assumptions regarding reactor data, as indicated in the legend. For comparison, we show as a grey-shaded area the region obtained in our previous solar + KamLAND data analysis. Right: the region allowed at 90, 95, 99 and 99.73% CL in our recommended analysis of solar + KamLAND data including SBL reactor results.

disappears and $\theta_{13} = 0$ is consistent within 1σ. This can be understood from figure 5, which shows that the SBL reactor experiments pull down the flux predictions, leaving less room for a suppression at 1 km due to θ_{13}. The upper limit on $\sin^2\theta_{13}$ is very similar to old and new fluxes when SBL data are included, irrespective of whether the normalization is left free or not. These results are in agreement with [6]. Figure 6 (right) shows the correlation between $\sin^2\theta_{13}$ and the flux normalization f with and without SBL experiments.

To summarize this section, we emphasize that owing to the tension between the new flux predictions and the SBL oscillation data, depending on whether or not the SBL reactors are included in the fit, different results on the extracted value of θ_{13} are obtained. This will indeed be seen in our subsequent fit results; see, for example, section 5.

4. Solar + KamLAND analysis in the light of new reactor fluxes

The release of new solar data from the second and third phases of the SK [11, 12] experiment, new data from the reactor experiment KamLAND [14] and the new predictions for the reactor anti-neutrino fluxes make a revision of the solar + KamLAND neutrino data analysis necessary. In figure 7, we show the 2σ allowed region from the solar + KamLAND neutrino data using different assumptions in the reactor data analysis, such as including or not including the SBL data or the use of a free normalization factor for the reactor anti-neutrino fluxes. In all cases the shift of the allowed region is not very significant, and the best-fit point values vary between 0.304 and 0.320 for $\sin^2\theta_{12}$, whereas the solar mass splitting Δm^2_{21} goes from 7.59 to 7.64×10^{-5} eV^2. The variation in $\sin^2\theta_{12}$ is slightly larger, because this parameter is correlated with the shift of $\sin^2\theta_{13}$, as shown in figure 8.

In the left panel of figure 8 we show the 2σ allowed regions in the $\sin^2\theta_{12}$–$\sin^2\theta_{13}$ plane for different choices of the reactor data analysis. For comparison, we also show in grey the 2σ allowed region obtained from solar data alone. In the right panel of figure 8, we show the

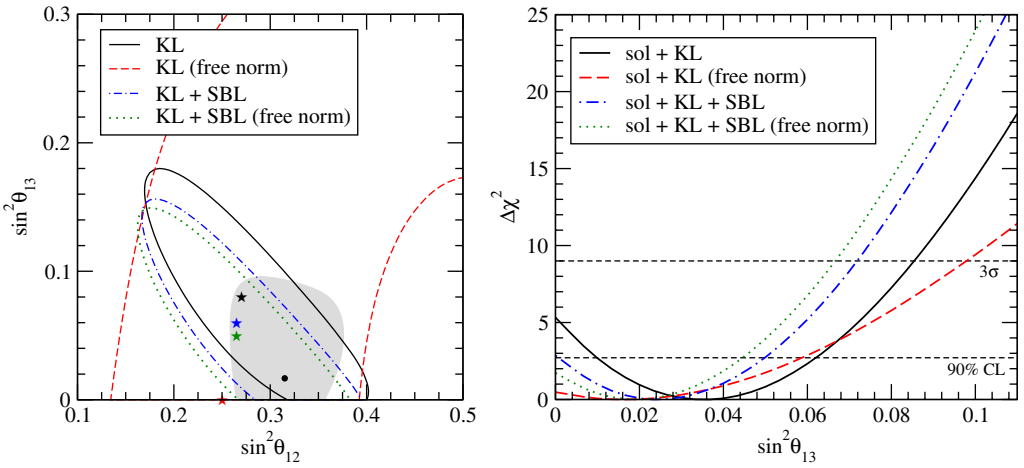

Figure 8. Left: 2σ allowed region in the $\sin^2\theta_{12}$–$\sin^2\theta_{13}$ plane obtained from KamLAND data using different assumptions regarding the reactor data analysis. For comparison, we also show the 2σ allowed region from solar data alone (grey-shaded area). Right: $\Delta\chi^2$ as a function of $\sin^2\theta_{13}$ for the solar + KamLAND data analysis under the same assumptions as in the left panel.

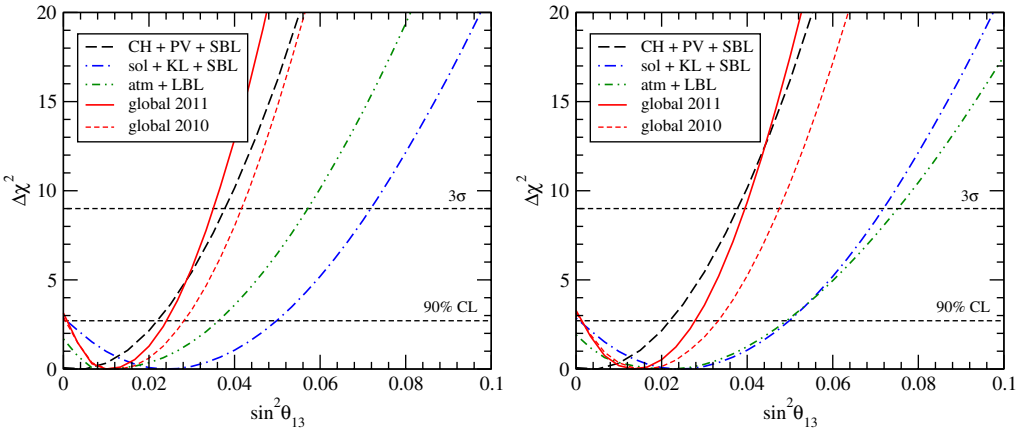

Figure 9. Constraints on $\sin^2\theta_{13}$ from different data sets, shown for NH (left) and IH (right). The curves labelled 'CH+PV+SBL' include the Chooz, Palo Verde and SBL reactor experiments, 'solar+KL+SBL' include solar, KamLAND and SBL reactor data, and 'atm + LBL' include SK atmospheric data MINOS (disappearance and appearance) and K2K. The results of our previous 2010 analysis are also shown for comparison.

constraints on θ_{13} from the combination of solar and KamLAND data. For the global neutrino oscillation fit presented in the following, we will use the analysis of KamLAND+SBL data without free normalization, labelled as 'sol + KL + SBL' in figure 8. In this case, we obtain the following best-fit value for θ_{13}:

$$\sin^2\theta_{13} = 0.023^{+0.016}_{-0.013} \quad \text{(solar + KamLAND)} \tag{3}$$

with $\Delta\chi^2(\sin^2\theta_{13}=0)=2.9$, and therefore a 1.7σ hint for $\theta_{13}\neq 0$ coming from the solar sector. Compared with our previous analysis [1], the inclusion of new solar and KamLAND data and the new reactor fluxes results in a similar best-fit value for the θ_{13} mixing angle (before, we obtained $\sin^2\theta_{13}=0.022$), but a slightly larger significance for nonzero θ_{13} (before: $\Delta\chi^2=2.2$). The origin of this is mainly the preference of KamLAND data for a nonzero θ_{13}, visible in the left panel of figure 8. For KamLAND, θ_{13} acts mainly as an overall reduction of the spectrum, and therefore, the increased event rate due to the new reactor fluxes can be compensated for by a nonzero θ_{13} in KamLAND.

Let us note that Mention *et al* [6] have also investigated the implication for θ_{13} of reactor neutrino data in the light of the new fluxes. Our results are in reasonable agreement with their results, although minor quantitative differences exist, presumably due to the different data used as well as the different analysis strategies.

5. Global three-neutrino analysis and status of θ_{13}

Let us now present the results of the global analysis combining all data mentioned in the previous sections[5]. As default for the reactor analysis, we use the new anti-neutrino flux predictions and include in the analysis the SBL reactor experiments as discussed in section 3.

Figure 9 shows the χ^2 profile as a function of $\sin^2\theta_{13}$ for various data samples. In the upper part of table 1, we display the corresponding best-fit values and the significance for $\theta_{13}>0$. In our standard recommended analysis (new reactor fluxes, SBL reactors included), we find no significant hint from Chooz and Palo Verde data, but the 1.7σ hint from solar + KamLAND (see section 4) and the 1.3σ (1.4σ for IH) hint from atmospheric + MINOS data (see section 2.3) combine to a global hint at 1.8σ for NH and IH, to be compared with the 1.5σ obtained in our previous analysis. In the lower part of table 1, we discuss how this result depends on details of the reactor neutrino analysis. If SBL data are not used in the fit the significance for $\theta_{13}>0$ is pushed close to 3σ because, as discussed in section 3, in this case Chooz and Palo Verde prefer $\theta_{13}>0$ at about 90% CL. However, in the flux-free reactor analysis as well as with the old reactor fluxes, the hint decreases to about 1.4σ and 1.8σ, respectively. The entry in the table labelled 'global without reactors' comes from atmospheric and solar neutrinos plus data from the MINOS long-baseline experiment. Therefore, these results are independent of any ambiguity due to reactor fluxes, and we observe that a nontrivial limit on θ_{13} emerges even in this case. Let us mention that here we always assume the AGSS09 solar model [33]. As discussed previously [1, 3] there is a minor dependence of the hint for θ_{13} on this assumption.

Figure 10 illustrates the interplay of the various data sets in the plane of $\sin^2\theta_{13}$ and Δm^2_{31}. In table 2, we summarize the determination of neutrino oscillation parameters for our reference default reactor analysis. As discussed in section 4, the impact of this choice on the leading oscillation parameters is small. We find that inverted hierarchy gives a slightly better fit, but with only $\Delta\chi^2=0.54$ with respect to the best fit in normal hierarchy.

6. Summary and conclusions

We have presented an updated global fit to the world's neutrino oscillation data. A recent re-evaluation of the anti-neutrino fluxes emitted in nuclear power plants [5] introduces some

[5] See also [1, 2] for previous experimental references.

Table 1. The best-fit values for $\sin^2\theta_{13}$ with 1σ errors, the significance of the $\theta_{13} > 0$ hint and the upper bound on $\sin^2\theta_{13}$ at 3σ for different data samples and for different reactor neutrino data assumptions. For a given global analysis the upper (lower) numbers refer to normal (inverted) neutrino mass hierarchy. We always use the new reactor fluxes [5], except for the row labelled 'old fluxes', which uses the previous results [22]. The row labelled 'free norm' assumes a free reactor anti-neutrino flux normalization.

	$\sin^2\theta_{13}$	$\Delta\chi^2(\theta_{13}=0)$	3σ bound
Solar+KamLAND+SBL	$0.023^{+0.016}_{-0.013}$	2.9 (1.7σ)	0.072
Chooz+Palo Verde+SBL	$0.005^{+0.010}_{-0.020}$	0.07 (0.26σ)	0.038
Atmospheric+MINOS	$0.010^{+0.016}_{-0.008}$	1.7 (1.3σ)	0.057
	$0.020^{+0.018}_{-0.015}$	1.9 (1.4σ)	0.075
Global without reactors	$0.013^{+0.014}_{-0.009}$	2.3 (1.5σ)	0.053
	$0.020^{+0.015}_{-0.012}$	2.7 (1.6σ)	0.065
Global with SBL	$0.010^{+0.009}_{-0.006}$	3.1 (1.8σ)	0.035
	$0.013^{+0.009}_{-0.007}$	3.3 (1.8σ)	0.039
Global with SBL (free norm)	$0.007^{+0.009}_{-0.005}$	2.0 (1.4σ)	0.032
	$0.010^{+0.009}_{-0.007}$	1.9 (1.4σ)	0.037
Global without SBL	$0.020^{+0.010}_{-0.008}$	7.0 (2.6σ)	0.048
	$0.027^{+0.009}_{-0.010}$	8.0 (2.8σ)	0.054
Global without SBL (old fluxes)	$0.012^{+0.010}_{-0.007}$	2.9 (1.7σ)	0.042
	0.017 ± 0.010	3.2 (1.8σ)	0.048

ambiguity in the results obtained for the mixing angle θ_{13}. Since the new predictions are in slight disagreement with data from SBL reactor experiments, with $L \lesssim 100$ m, it becomes necessary to include these data in the fit. A flux-free analysis of SBL data prefers an offset of the reactor neutrino flux of about 6% from the predicted value with a significance of about 2.5σ. Taken at face value this might indicate either some unaccounted for systematic effect (either in the new calculations or in the reactor data) or even the presence of some kind of new physics such as sterile neutrino oscillations with $\Delta m^2 \sim 1\,\mathrm{eV}^2$ [6]. Here we stick to the three-flavour framework; the sterile neutrino hypothesis will be discussed elsewhere [34].

Despite this hint for a deviation of the observed reactor anti-neutrino flux from its prediction, the GOF of the SBL reactor neutrino data to the new fluxes is still very good ($\chi^2 = 13$ for 12 degrees of freedom). Motivated by this result, we adopt as our recommended default analysis the new fluxes and include the SBL data in the fit. In this way we obtain a hint for $\theta_{13} > 0$ at 1.8σ, coming from a preference for a finite θ_{13} from KamLAND data combined with a somewhat weaker hint from the joint analysis of atmospheric + MINOS data. Table 1

Table 2. A summary of neutrino oscillation parameters. For Δm^2_{31}, $\sin^2\theta_{23}$ and $\sin^2\theta_{13}$ the upper (lower) row corresponds to normal (inverted) neutrino mass hierarchy. We assume the new reactor anti-neutrino fluxes [5] and include SBL reactor neutrino experiments in the fit.

Parameter	Best fit $\pm 1\sigma$	2σ	3σ
Δm^2_{21} (10^{-5} eV^2)	$7.59^{+0.20}_{-0.18}$	7.24–7.99	7.09–8.19
Δm^2_{31} (10^{-3} eV^2)	2.45 ± 0.09	2.28–2.64	2.18–2.73
	$-(2.34^{+0.10}_{-0.09})$	$-$(2.17–2.54)	$-$(2.08–2.64)
$\sin^2\theta_{12}$	$0.312^{+0.017}_{-0.015}$	0.28–0.35	0.27–0.36
$\sin^2\theta_{23}$	0.51 ± 0.06	0.41–0.61	0.39–0.64
	0.52 ± 0.06	0.42–0.61	
$\sin^2\theta_{13}$	$0.010^{+0.009}_{-0.006}$	$\leqslant$0.027	$\leqslant$0.035
	$0.013^{+0.009}_{-0.007}$	$\leqslant$0.031	$\leqslant$0.039

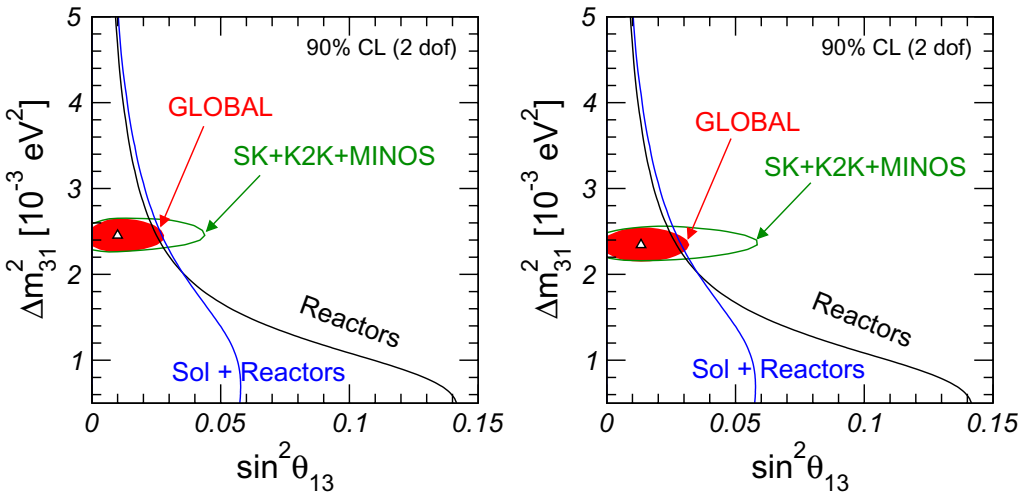

Figure 10. Illustration of the interplay of the global data on the $\sin^2\theta_{13}$ bound. Left: NH; right: IH.

shows in detail how the global result depends on the assumptions regarding the reactor neutrino analysis, yielding hints for $\theta_{13} > 0$ ranging between 1.4σ and 2.8σ, with best-fit values between $\sin^2\theta_{13} = 0.007$ and 0.027. This somewhat ambiguous situation regarding θ_{13} emerges from the slight tension between the new reactor flux predictions and existing data. It will be interesting to see how the upcoming results from new reactor and accelerator experiments searching for θ_{13} will contribute to resolving the issue; see [19] for an overview and references.

The main results of our recommended default analysis of three-neutrino oscillation parameters are summarized in table 2 and in the right panels of figures 3 and 7 for the leading 'atmospheric' and 'solar' oscillation parameters, as well as in figure 10 for the mixing angle θ_{13}.

Acknowledgments

We thank Ed Kearns for discussions during Neutrino 2010 and especially for providing us with the Super-Kamiokande Collaboration χ^2 map given in [13]. We also thank T Lasserre, M Fechner and D Lhuillier for communication on the SBL reactor analysis in relation to the new fluxes. This work was supported by the Spanish grants FPA2008-00319/FPA, MULTIDARK Consolider CSD2009-00064 and PROMETEO/2009/091 and by the EU network UNILHC (PITN-GA-2009-237920). MT acknowledges financial support from CSIC under the JAE-Doc programme. This work was partly supported by the Transregio Sonderforschungsbereich TR27 'Neutrinos and Beyond' der Deutschen Forschungsgemeinschaft.

References

[1] Schwetz T, Tortola M A and Valle J W F 2008 *New J. Phys.* **10** 113011 (arXiv:0808.2016v3 [hep-ph])
[2] Maltoni M, Schwetz T, Tortola M A and Valle J W F 2004 *New J. Phys.* **6** 122 (arXiv:hep-ph/0405172)
[3] Gonzalez-Garcia M C, Maltoni M and Salvado J 2010 *J. High Energy Phys.* JHEP1004(2010)056 (arXiv:1001.4524 [hep-ph])
[4] Lisi T E 2011 *Neutrino Telescopes (Venice, Italy, 15–8 March 2011)* http://neutrino.pd.infn.it/Neutel2011/
[5] Mueller T A *et al* 2011 arXiv:1101.2663 [hep-ex]
[6] Mention G *et al* 2011 arXiv:1101.2755 [hep-ex]
[7] Adamson P *et al* [The MINOS Collaboration] 2010 arXiv:1006.0996 [hep-ex]
[8] Vahle P [The MINOS Collaboration] 2010 Talk at the *Neutrino 2010 Conf. (Athens, Greece)*
[9] Adamson P *et al* [The MINOS Collaboration] 2011 arXiv:1103.0340 [hep-ex]
[10] Adamson P *et al* [The MINOS Collaboration] 2011 arXiv:1104.0344 [hep-ex]
[11] Cravens J P *et al* [Super-Kamiokande Collaboration] 2008 *Phys. Rev.* D **78** 032002 (arXiv:0803.4312 [hep-ex])
[12] Abe K *et al* 2010 arXiv:1010.0118 [hep-ex]
[13] Wendell R *et al* [Super-Kamiokande Collaboration] 2010 *Phys. Rev.* D **81** 092004 (arXiv:1002.3471 [hep-ex])
[14] Gando A *et al* 2010 arXiv:1009.4771 [hep-ex]
[15] Takeuchi Y [Super-Kamiokande Collaboration] 2010 Talk at the *Neutrino 2010 Conf. (Athens, Greece)*
[16] Huber P, Kopp J, Lindner M, Rolinec M and Winter W 2007 *Comput. Phys. Commun.* **177** 432 (arXiv: hep-ph/0701187)
[17] Maltoni M and Schwetz T 2003 *Phys. Rev.* D **68** 033020 (arXiv:hep-ph/0304176)
[18] Adamson P *et al* [MINOS Collaboration] 2009 *Phys. Rev. Lett.* **103** 261802 (arXiv:0909.4996 [hep-ex])
[19] Mezzetto M and Schwetz T 2010 *J. Phys. G: Nucl. Part. Phys.* **37** 103001 (arXiv:1003.5800 [hep-ph])
[20] Goswami S and Smirnov A Y 2005 *Phys. Rev.* D **72** 053011 (arXiv:hep-ph/0411359)
[21] Fogli G L, Lisi E, Marrone A, Palazzo A and Rotunno A M 2008 *Phys. Rev. Lett.* **101** 141801 (arXiv:0806.2649 [hep-ph])
[22] Schreckenbach K *et al* 1985 *Phys. Lett.* B **160** 325–30
Hahn A A *et al* 1989 *Phys. Lett.* B **218** 365–68
Von Feilitzsch F, HahnA A and Schreckenbach K 1982 *Phys. Lett.* B **118** 162–6
[23] Vogel P *et al* 1981 *Phys. Rev.* C **24** 1543–53
[24] Declais Y *et al* 1994 *Phys. Lett.* B **338** 383
[25] Kuvshinnikov A A *et al* 1991 *JETP Lett.* **54** 253
Kuvshinnikov A A *et al* 1991 *Sov. J. Nucl. Phys.* **52** 300
[26] Declais Y *et al* 1995 *Nucl. Phys.* B **434** 503
[27] Vidyakin G S *et al* 1987 *Sov. Phys.—JETP* **66** 243
Vidyakin G S *et al* 1987 *Zh. Eksp. Teor. Fiz.* **93** 424

Vidyakin G S *et al* 1994 *JETP Lett.* **59** 390
Vidyakin G S *et al* 1994 *Pisma Zh. Eksp. Teor. Fiz.* **59** 364
[28] Kwon H *et al* 1981 *Phys. Rev.* D **24** 1097
[29] Zacek G *et al* 1986 *Phys. Rev.* D **34** 2621
[30] Apollonio M *et al* [CHOOZ Collaboration] 2003 *Eur. Phys. J.* C **27** 331 (arXiv:hep-ex/0301017)
[31] Boehm F *et al* 2001 *Phys. Rev.* D **64** 112001 (arXiv:hep-ex/0107009)
[32] Bilenky S M, Giunti C and Grimus W 1998 *Eur. Phys. J.* C **1** 247 (arXiv:hep-ph/9607372)
Barger V D *et al* 2000 *Phys. Lett.* B **489** 345–52 (arXiv:hep-ph/0008019)
Peres O L G and Smirnov A Y 2001 *Nucl. Phys.* B **599** 3 (arXiv:hep-ph/0011054)
Grimus W and Schwetz T 2001 *Eur. Phys. J.* C **20** 1–11 (arXiv:hep-ph/0102252)
Maltoni M, Schwetz T and Valle J W F 2001 *Phys. Lett.* B **518** 252 (arXiv:hep-ph/0107150)
[33] Serenelli A, Basu S, Ferguson J W and Asplund M 2009 arXiv:0909.2668 [astro-ph.SR]
[34] Kopp J, Maltoni M and Schwetz T 2011 arXiv:1103.4570 [hep-ph]